

Coating of Ordered Large-Pore Mesoporous Silica with TiO₂ Nanoparticles and Evaluation of Its Photocatalytic Activity

A. HAGHIGHATZADEH^a, B. MAZINANI^b AND M. ABDOLAHPOUR SALARI^{c,*}

^aPhysics Group, Department of Sciences, Ahvaz Branch, Islamic Azad University, P.O. Box 61349-68875, Ahvaz, Iran

^bDepartment of Materials Engineering, Malayer University, Malayer, Iran

^cDepartment of Physics, Science Faculty, Ataturk University, 25240, Erzurum, Turkey

In this work, at first large pore size SiO₂ mesostructure was prepared using amphiphilic triblock copolymer (P123) as a template, tetraethyl orthosilicate (TEOS) as Si source and hexane as micelle expander by hydrothermal procedure. Separately, a stable transparent titania sol was synthesized using titanium isopropoxide (TTIP) as titanium source. Then achieved mesoporous silica structure was stirred in the titania sol resulting in formation of a titanium dioxide anatase layer on the silica structure. The sample was characterized with wide angle X-ray diffraction, N₂ adsorption-desorption analysis, X-ray photoelectron spectroscopy, field-emission scanning electron microscopy, and energy dispersive X-ray spectroscopy maps of silicon and titanium. The photocatalytic performance of prepared composite material was evaluated using UV-vis spectroscopy as well. The prepared material showed much higher photodegradation of methyl blue (MB) than commercial P-25 which was attributed to high surface area (290 m²/g), anatase phase, small crystallite size and accessible pores.

DOI: [10.12693/APhysPolA.132.420](https://doi.org/10.12693/APhysPolA.132.420)

PACS/topics: mesoporous, titania, silica, photocatalytic activity

1. Introduction

Over the last few years, TiO₂ as a photocatalyst has attracted researchers attention because of its competitive price, superior chemical stability, and nontoxicity [1–4]. However, limited photoactivity of titanium oxide can be considered as an obstacle to the industrial usage. As photoactivity of TiO₂ is a surface reaction, achieving of higher surface area is an effective solution [5]. Although, using of TiO₂ nanoparticle seems to be an appropriate solution, problem encountered in separation of ultrafine TiO₂ particles is a major hurdle.

Another alternative to overcome the problem is using mesoporous TiO₂ structure with high surface area and large particle size [6–8]. However, synthesis of mesoporous TiO₂ often encounter several difficulties such as crystal phase control and mesostructure control [9–13].

Recently using of mesoporous silica as a host structure to synthesis mesoporous SiO₂-TiO₂ has been reported as a suitable solution [1, 14, 15]. High surface area of achieved materials and formation of Ti-O-Si bonds which prevent crystal growth, increase photocatalytic efficiency.

Although synthesis of mesoporous SiO₂-TiO₂ has been widely studied, increase of photoactivity of prepared mesostructure TiO₂-SiO₂ materials is a burning issue yet. In this paper, at first we synthesized large pore mesoporous SiO₂ as host structure in order to reduce pore plugging by TiO₂ nanoparticles. Then anatase nanoparticles were deposited on the surface and pores of the mesoporous silica structure.

2. Experimental

2.1. Synthesis procedure

At first 2.4 g of P123 (Aldrich) was dissolved in 84 ml HCl solution (1.3 M). Then 0.027 g NH₄F (Merck) was added to the solution. After that the solution was stirred for 2 h at 15 °C. Next, a mixture of 5.5 ml tetraethoxysilane (Merck) and 15 ml hexane (Baker) was introduced to the solution. The solution was stirred for 24 h at 15 °C. The prepared mixture was treated hydrothermally at 100 °C for 48 h. The precipitate was filtered, washed, and heat treated (sample S1).

After that, a transparent and stable titania sol was prepared by dissolving of 2.5 g PEG, 2.5 g DEG, and 5 g TTIP (Aldrich) in 40 ml of ethanol with stirring.

The prepared silica host structure was added to transparent titania sol with stirring. After 5 h it was filtered, dried and calcined at 600 °C. The prepared oxide material was denoted as S2.

2.2. Characterization

Crystal structure of the materials was tested by X-ray diffraction (XRD). The XRD patterns were recorded with a Bruker powder X-ray diffractometer using a Cu K_α ranging from 20° to 80° and 40 mA. The morphology and EDX analysis of the sample was characterized by scanning electron microscopy (SEM, LEO-1525) with an accelerating voltage of 20 kV. The surface area of all the sample was characterized by nitrogen adsorption-desorption (BET) using the Autosorb-1 from Quantachrome Instruments. X-ray photoelectron spectroscopy (XPS) spectra were recorded with Omicron Nanotechnology (ELS5000) system using Al K_α radiation at a base pressure below 5.5 × 10⁻⁹ Torr.

*corresponding author; e-mail: maryam_salari2@yahoo.com

Methylene blue degradation under UV light (mercury lamp, 125 W) was used to evaluate photocatalytic efficiency. 30 mg of prepared composite material was dispersed in 100 mL MB solution of concentration 40 mg/L. XPS spectra were recorded with Omicron Nanotechnology (ELS5000) system using Al K_{α} radiation at a base pressure below 5.5×10^{-9} Torr. The concentration of MB in the mixture was determined by UV-vis spectrometry (Lambda 25 Perkin-Elmer) after centrifuging.

3. Results and discussion

XRD pattern of the prepared sample is shown in Fig. 1. As it can be seen, anatase crystals are the only presented phase. It is reported that phase transformation from anatase to rutile is around 400–500 °C during calcination process. However, anatase is the only detectable phase until at least 600 °C in the present sample due to formation of Ti–O–Si bonds according to XPS results (Fig. 2). Ti–O–Si bonds can inhibit phase transformation and consequently higher photocatalytic activity can be achieved. The average crystallite size of anatase is 5 nm calculated by the Scherrer equation, as follows:

$$S = \frac{0.9\lambda}{\beta \cos \theta}, \quad (1)$$

where S is the crystallite size, λ is the wavelength of the X-ray radiation which is 0.154 nm for Cu K_{α} , β is the full width at half maximum of the diffraction peak, and θ is the diffraction angle.

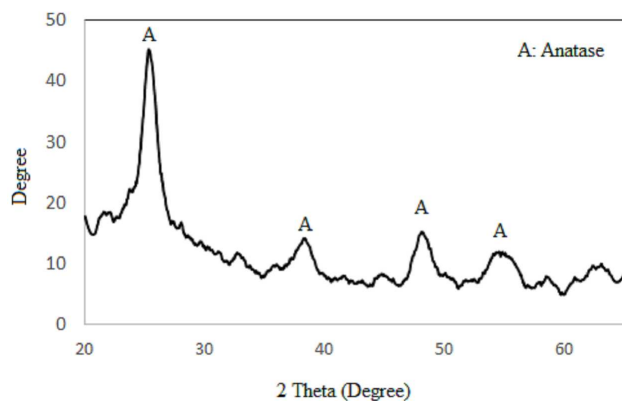


Fig. 1. XRD pattern of the sample.

The XPS spectra of the sample is presented in Fig. 2. The profiles of the samples can be fitted by three Lorentzian curves. The peaks around 533.5 eV and 530.5 eV are related to oxygen in Si–O–Si and Ti–O–Ti bonds, respectively [16]. In addition, a peak at an intermediate binding energy (532.2 eV) can be assigned to oxygen in Si–O–Ti. It has been proved that the existence of Ti–O–Si bond can increase photocatalytic performance because of an increase in surface acidity.

SEM pattern of the rod-like particle is shown in Fig. 3. Also, EDX maps of the particle are presented in Fig. 3b and c. Figure 3b and c represents that Si and Ti are distributed homogeneously in the particle.

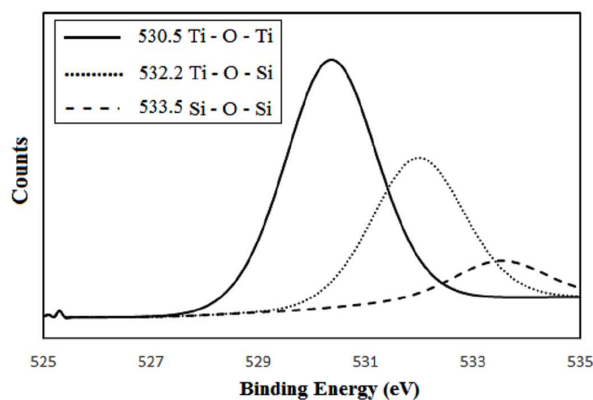


Fig. 2. XPS spectra of silica-titania sample.

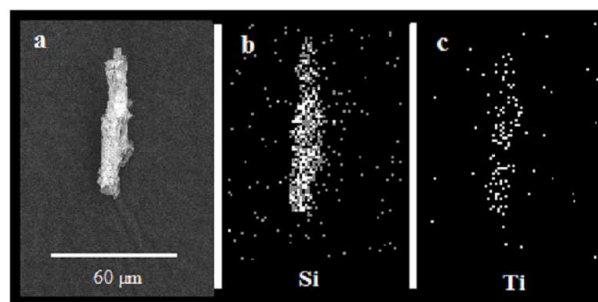


Fig. 3. SEM micrograph (a) and EDX maps of silicon (b), and titanium (c) of sample.

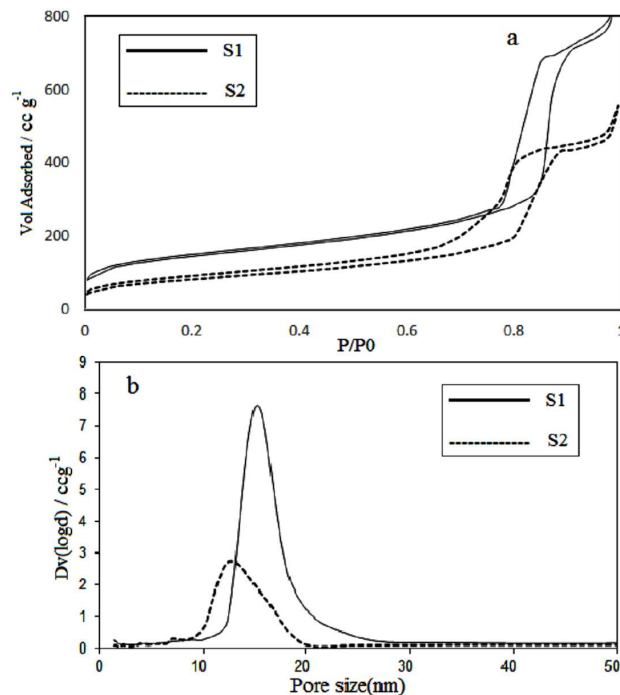


Fig. 4. (a) Nitrogen sorption isotherms and (b) pore size distribution calculated from adsorption branch of the samples.

The N₂ adsorption–desorption isotherms and the corresponding pore size distribution of the samples were calculated from the adsorption branch of N₂ isotherm and can be seen in Fig. 4a and b, respectively. The isotherms can be categorized as type IV with H1 hysteresis loop according to IUPAC classification. Surface area and pore volume of host structure (sample S1) were calculated as 497 m²/g and 1.33 cm³/g, respectively. After impregnation of TiO₂ (sample S2), surface area and pore volume declined to 293 m²/g and 0.86 cm³/g, respectively, which results beside elemental map of the sample (Fig. 3) and XPS result (Fig. 2) can prove deposition of anatase particles inside the channels and surface of silica host structure.

The degradation performance of MB by TiO₂ can be related to several factors, including electron–hole recombination, phase composition (anatase or rutile), surface area, degree of crystallinity and particle size of TiO₂. Two factors can be mentioned for reducing of MB concentration by TiO₂ particles in an aqueous solution: (i) the adsorption of MB on the surface of sample and (ii) photodegradation of MB. In order to estimate each of them the suspension was stirred for 30 min in dark condition in advance. Then the sample was stirred under UV light for 60 min and the results are shown in Fig. 5.

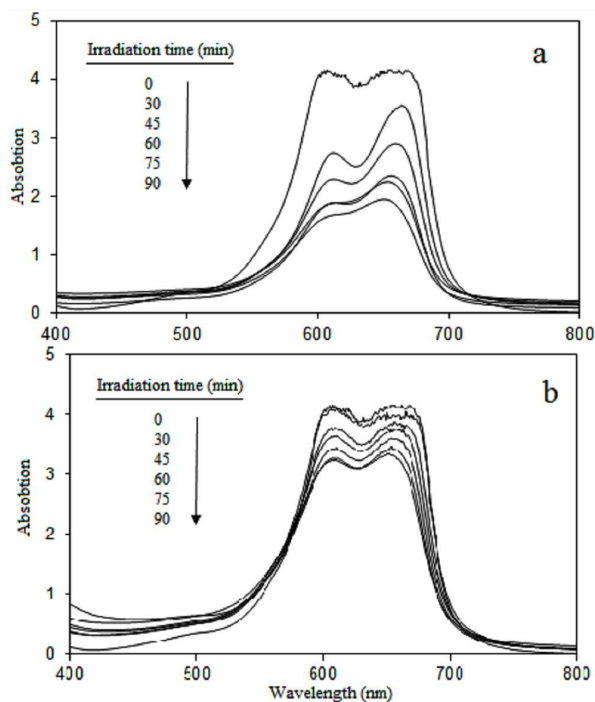


Fig. 5. 5: MB degradation by sample S2 (a) and P25 (b).

Photocatalytic efficiency can be calculated according to the following equation [17]:

$$E = \frac{C_0 - C}{C_0} \times 100\%, \quad (2)$$

Where C_0 is the initial concentration of the MB solution and C is the final concentration after illumination and E

is the photocatalytic efficiency. According to Eq. (2), E is calculated as 53.7% for sample S2, while this value was estimated as 19.3% for commercial P25 (about 50 m²/g). High photoactivity of the mesoporous TiO₂–SiO₂ can be related to high surface area, presence of Ti–O–Si bonds and existence of anatase crystal phase in sample.

4. Conclusion

In summary, at first ordered mesoporous SiO₂ with large pores was synthesized by introducing TTIP as Ti source and hexane as micelle expander into solution at low synthesis temperature ($T = 15^\circ\text{C}$). Then the prepared host structure was stirred in a stable titania solution. Results show that TiO₂ particles were deposited on the surface and channels of silica structure successfully. Photocatalytic efficiency of the prepared sample was around twice more than of Degussa P25.

References

- [1] B. Mazinani, A. Beitollahi, S. Radiman, A.K. Masrom, S.M. Ibrahim, J. Javadpour, F.M.D. Jamil, *J. Alloys Comp.* **519**, 72 (2012).
- [2] I. Karabay, S. Aydm Yüksel, F. Ongül, S. Öztürk, M. Ashi, *Acta Phys. Pol. A* **121**, 265 (2012).
- [3] M. Tuncer, B. Ozdemir, *Acta Phys. Pol. A* **125**, 608 (2014).
- [4] Bahşi Oral Zehra Banu, *Acta Phys. Pol. A* **127**, 1314 (2015).
- [5] N. Xu, Z. Shi, Y. Fan, J. Dong, J. Shi, M.Z.-C. Hu, *Ind. Eng. Chem. Res.* **38**, 373 (1999).
- [6] T. An, J. Liu, G. Li, S. Zhang, H. Zhao, X. Zeng, G. Sheng, J. Fu, *Appl. Catal. A Gen.* **350**, 237 (2008).
- [7] J. Du, Z. Liu, Z. Li, B. Han, Y. Huang, Y. Gao, *Micropor. Mesopor. Mater.* **83**, 19 (2005).
- [8] S.M. Ibrahim, A.K. Masrom, B. Mazinani, S. Radiman, F.M. Jamil, A. Beitollahi, N. Negishi, N. Yahya, *Res. Chem. Intermed.* **39**, 1003 (2013).
- [9] P. Yang, D. Zhao, D.I. Margolese, B.F. Chmelka, G.D. Stucky, *Nature* **396**, 152 (1998).
- [10] B. Tian, X. Liu, B. Tu, C. Yu, J. Fan, L. Wang, S. Xie, G.D. Stucky, D. Zhao, *Nat. Mater.* **2**, 159 (2003).
- [11] M.D. Prez, E. Otal, S.A. Bilmes, G.J.A.A. Soler-Illia, E.L. Crepaldi, D. Grosso, C. Sanchez, *Langmuir* **20**, 6879 (2004).
- [12] S.Y. Choi, B. Lee, D.B. Carew, M. Mamak, F.C. Peiris, S. Speakman, N. Chopra, G.A. Ozin, *Adv. Funct. Mater.* **16**, 1731 (2006).
- [13] X. Ding, X. Liu, *J. Mater. Res.* **13**, 2556 (1998).
- [14] B. Mazinani, A.K. Masrom, A. Beitollahi, R. Luque, *Ceram. Int.* **40**, 11525 (2014).
- [15] B. Mazinani, A. Beitollahi, A.K. Masrom, N. Yahya, T.S.Y. Choong, S.M. Ibrahim, J. Javadpour, *Res. Chem. Intermed.* **38**, 1733 (2012).
- [16] Z.L. Hua, J.L. Shi, L.X. Zhang, M.L. Ruan, J.N. Yan, *Adv. Mater.* **14**, 830 (2002).
- [17] H.E. Byrne, W.L. Kostedt, J.M. Stokke, D.W. Mazyck, *J. Non-Cryst. Solids* **355**, 525 (2009).